

Coupling between Curvature and Molecule/Particle Orientation in Soft Condensed Matter Systems

Charles Nathan Melton

1 Introduction

Condensed matter is a very broad field of physics that concerns many different types of systems. Condensed matter physicists seek to understand how molecular level interactions affect the overall bulk properties of the system. Systems that condensed matter physicists study involve crystals, fluids, liquid crystals, lipid bilayers, superconductors, superfluids, just to name a few [1].

Not only is condensed matter a very broad field, but it is also quite interdisciplinary. Biologist, chemists, physicists, engineers, and mathematicians all study condensed matter systems. While the scientists seek to understand these systems and explain how they work, engineers take up the task of developing devices and technology that implements these systems. LCD TVs are one great example of a benefit to society that is the product of the study of condensed matter systems.

Soft condensed matter systems are very temperature dependent. Liquid crystals, for example, exhibit very unique phase behavior. While most materials exhibit three main phases (crystalline, liquid, and gas), liquid crystals have phase behavior that is a combination of both liquid and crystalline, thus the name liquid crystal. One such phase is known as the nematic phase, where the molecules experience directional order, yet behave like a liquid. The energy required to have the liquid crystal experience these in-between phase changes is on the order of $k_B T$ [2]. Disclination lines, or defects, may occur in the liquid crystal. A defect occurs when liquid crystal molecules that are oriented in different directions meet.

While soft condensed matter systems are subject to phase behavior on small energy scales, there is another aspect that is important in understanding these systems: curvature. Principle curvature is defined as a tensor on a point of a surface. A surface is defined as a $(d - 1)$ manifold in d space. For a 2D curve, the curvature tensor is a scalar defined as

$$C = \frac{1}{R} \tag{1.1}$$

where R is the radius of a circle that follows the curve [1], as shown in Figure 1.

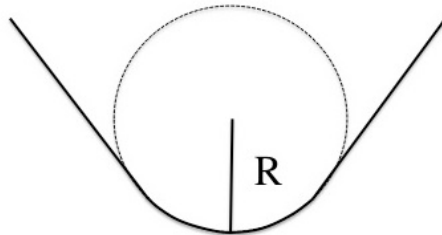


Figure 1: Diagram of the definition of curvature.

If we consider a 2D membrane, we may have curvature in both the x and y directions. C_1 and C_2 are defined the same as Equation (1.1). When 2D membrane is curved, we can express its elastic energy as

$$f = \int \left[\frac{\kappa}{2} (2H + c_0)^2 + \bar{\kappa} K \right] dA \quad (1.2)$$

where $H = \frac{C_1 + C_2}{2}$ is the mean curvature, $K = C_1 C_2$ is the gaussian curvature, and κ is the elastic constant of the membrane [2].

Certain behaviors of soft matter systems depend on curvature. Lipid bilayer kinetics have been shown to be affected by their curvature. For example, the fusion rate of vesicles has been shown to decrease as bilayer curvature and vesicle size increases [3]. Also, the defects observed in liquid crystals are a function of curvature. For example, bipolar defects are formed in nematic droplets due to the molecules following the surface of the droplet towards the poles, and the molecules meet at the poles all pointing in different directions [4].

The work discussed in this proposal is to study the effects on inducing curvature in 2D and 3D soft condensed matter systems. The systems to be explored are Giant Unilamellar Vesicles (GUVs), liquid crystal droplets, and soft matter structures formed by particles at the interface of oil and water, also known as Pickering emulsions. To induce a curvature to the GUVs and liquid crystal droplets, a dual-fiber optical trap will be implemented. The forces from the optical beams coming from the fibers will induce a stretching of the droplet, and different properties of the system can be extracted. Such topics to be studied are elastic moduli of the GUVs, possible reordering of lipid phase domains, the stretching of a nematic droplet and the possible rearrangement of disclinations. For the emulsions, the possible

rearrangement of surface defects will be studied, as well as curvature generation due to particles lying on the interface between oil and water.

The stretching of GUVs and liquid crystal droplets will lead to a better understanding of the coupling between particle/molecule orientation and curvature in soft condensed matter systems. GUV stretching will lead to a better understanding of the role of curvature in lipid sorting, which is the rearrangement of lipids in the membrane as a function of their surroundings, such as curvature. For liquid crystals, droplet studies are beneficial to further industrial applications of PDLC devices, such as displays and shutters. For particles on oil-water interfaces, the techniques used to study the particle layout can be used for other condensed matter systems when particle/molecule location is needed to be known. All these possibilities lead to the reasoning behind studying the link between curvature and molecule/particle orientation.

2 Overall Goals

What happens when one induces curvature changes to soft matter systems? How does the overall bulk system respond? How does the system change on the molecular level? System responses will be the result of many things: molecular composition, direction of applied forces, bulk material concentration, etc. My proposal goals are:

1. Study GUV mechanics as a function of lipid concentration, as well as lipid phase reorganization as a function of curvature

I will begin by first optimizing trapping conditions for GUVs. The first goal is to form GUVs in solutions that will help increase the trapping occurrences.

I will perform trapping experiments to obtain stress-strain profiles and bending elasticities as a function of lipid concentration.

I will perform trapping experiments on GUVs with different phase domains to study their relocation through the bilayer as a function of curvature.

2. Study the stretching of a nematic droplet

I will first form nematics droplets of a size between 20 and 50 μm for trapping.

I will then proceed to stretch the nematic droplets, obtaining mechanical properties of the droplet as a function of droplet size.

I will theoretically model the orientation of the molecules of a liquid crystal droplet, and predict their change in orientation as the curvature of the droplet is changed.

Finally, I will study how defect lines will change location as a function of curvature.

3. Study the relation between curved surfaces and particle orientation as the interface between oil and water

I will first create soft structures made of oil and water with particles at the interface. The particles will range by their aspect ratios.

With the structures made, I will obtain images via confocal microscopy.

Mapping of the surface as a function of particle orientation will then be done in collaboration with Professor Tim Atherton at Tufts University.

Finally, correlation functions of the particle layout from the images will be obtained the program Particle Tracker.

3 Dual-Fiber Optical Trap

Optical trapping has quite a history in studying soft condensed matter systems. One form of trapping called optical tweezers has been used to study systems such as the kinetics of kinesin motors [5] and stretching DNA [6]. While optical tweezers work well, they are quite invasive and may damage what is being tested. A non-invasive method would be ideal so as to not risk damaging the materials. The dual-fiber system was first used by Constable et. al. [7] to trap micron-sized particles using gaussian beams. Dual-beam traps have more recently become popular as a method of studying soft matter systems such as cells [8,9,11] and vesicles [10]. The dual-fiber optical trap was truly pioneered for bio-application by Guck to study the mechanical properties of red blood cells, as well as formulate mathematically the trapping physics [8].

3.1 Optical Trap Theory

When an object is placed in an optical trap, it is subjected to two main forces: scattering and gradient forces. The scattering force propagates in the direction of the laser beam (Figure 2). This force arises from the reflection off the surface of the trapped object, leading to a change in momentum of the photon. The gradient force arises due to refracted light through the dielectric micro-object [8,12]. The gradient force acts radially with respect to the beam profile, which for this experiment is a Gaussian profile. When the forces are in equilibrium, the object is said to be in a stable trap and held in place. But how can the object be stretched if there is no net force on the object? The answer to this question is momentum.

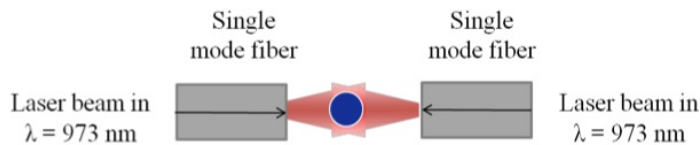


Figure 2: Diagram of trapping setup obtained from [12].

As one knows, light carries momentum. in the optical trap setup, the refractive index of the object being trapped should be higher than the solution the object is in. Since the light goes from a medium of low refractive index to one of higher, the momentum increases. However, momentum must be conserved [9]. This increase in momentum is felt by the surface of the object opposite of where the light entered, and since there was a change in momentum, there is a force felt. This force felt is given by

$$F = \frac{n_1 Q P}{c} \tag{3.1}$$

where n_1 is the refractive index of the solution the object is sitting in, P is the power of the incident light, Q is a factor that describes the amount of momentum that is transferred, and c is the speed of light.

3.2 Construction of the Optical Trap

The beauty of the dual-fiber optical trap lies in the simplicity of its construction, shown in Figure 3. Having a very cost effective design using cost effective materials allows for many traps to be constructed in a small amount of time. Construction begins by cutting a rectangular piece of plastic. The usual dimensions are roughly 4 cm by 2 cm, with a height of about 0.2 cm. A groove to hold the fibers is formed on the top side of the base by a wire pressed against the plastic, and heating the base via an electric current flowing through the wire. The optical fibers are then placed in the groove at the desired separation distance away from each other. The fibers are then sealed into place, and held down by a cover slip, which is also sealed. The laser used is a diode-pump laser (Bookham, Inc) and has a wavelength of 973 nm.

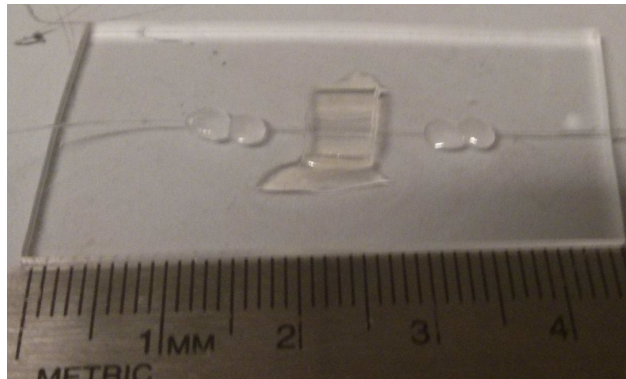


Figure 3: Constructed dual-beam optical trap

4 Experimental Plans and Methods

4.1 Project 1: GUV Stretching

4.1.1 Background and Theory

Giant Unilamellar Vesicles (GUVs) are lipid vesicles that commonly range from 5 to 20 μm in diameter. The bilayer produced by lipids is around 4 nm thick. The GUVs I produce are made specifically of phospholipids. Phospholipids are fatty acids that are composed of two main groups: a hydrophilic head group and a hydrophobic tail group, shown in Figure 4. The head is composed of phosphates called diglycerides, which are composed of glycerols, and usually a choline. The tails are hydrocarbon chains, and can be either saturated and unsaturated [2]. If there is double bond in the carbon chain, the lipid is unsaturated, and thus increases its flexibility.

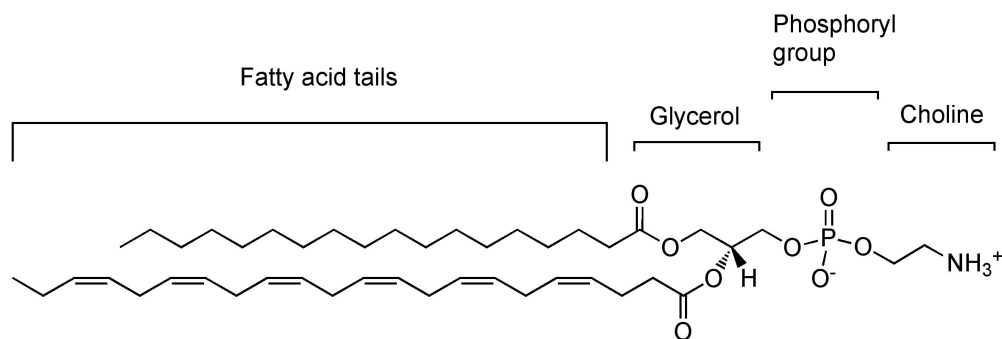


Figure 4: Diagram of a lipid molecule obtained from [2].

Lipids, as soft materials, can be subject to phase changes at certain temperatures. The most familiar GUV pictures, like shown in Figure 5a, show a very smooth bilayer composition. This is known as the fluid, or L_α phase. In this phase, the lipids are free to diffuse throughout the bilayer. The lipids are in this phase when they are above their melting temperature, T_m . Some lipids have a high melting temperature, and thus vesicles can be formed when the lipids are in what's known as a gel phase ($L_{\beta'}$) at room temperature. The gel phase occurs when there is long-range, in-plane ordering of the head groups. In this phase, diffusion is limited, and the tails are significantly tilted [2]. Compositions of different lipids can be made to produce vesicles showing both phases, as shown in Figure 5b.

Lipids and GUVs have been the subject of many studies into their phase behavior and physical properties. The diffusion behavior of lipids throughout a bilayer have been studied [14], as well organization behavior into a variety of shapes such as tubulals and disks [15]. A variety of studies of GUVs have been conducted as well. Phase diagrams, both binary and ternary, have been developed for a variety of lipids [16,17]. Curvature and molecular reorientation has been studied in flat membranes [18]. However, very little research has been

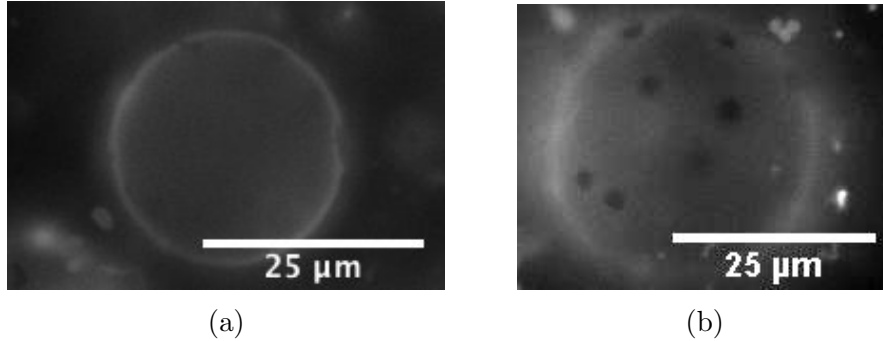


Figure 5: GUVs formed by electroformation. Both photos show GUVs made from a solution of 5 mM Sphingomyelin/DOPC (50 % by mol each) with 0.05 mol % Rh-PE (a) No visible phase separation. (b) Gel phase rafts visible on the surface of the membrane.

conducted on the deformation of GUVs through noninvasive means, as well as the reorganization of phase domains due to changes in curvature of the vesicles.

In addition to investigating lipid phase reorganization, lipid membrane mechanics are to be studied in a high elastic regime. It has been shown that for very small deformations of a lipid membrane, i.e. the straightening out of the thermal fluctuations of the membrane, the stress-strain relation is given by [19]

$$\epsilon = \frac{k_B T}{8\pi\kappa} \ln \frac{\sigma a^2}{\kappa\pi^2} \quad (4.1)$$

where κ is the bending modulus, a is a microscopic cutoff, and σ and ϵ are the common stress and strain, respectively. It will be interesting to see if this relation holds in the higher elastic regimes.

4.1.2 Methods and Proposed Work

To begin GUV production, stock lipids in chloroform are chosen and mixed accordingly to the desired molar ratios. Whether one lipid is being chosen to make the GUV, or two, the desired molarity is 10 mM. To ensure that proper phase separation of lipid phase domains occurs at room temperature when using two lipids, phase diagrams must be consulted, as well as choosing lipids whose melting temperatures are different. The common lipid chosen in all the prepared mixtures is 1,2-dioleoyl-sn-glycero-3-phosphocholine, or DOPC. When using two lipids, this will ensure GUVs are composed of both L_α and $L_{\beta'}$. For these mixtures, the lipid DPPE with Rhodamine (Rh-PE) is used for visualization under fluorescence microscopy. The usual concentration of Rh-PE is 0.05 mol %.

The GUVs are formed by a process called electroformation [8], with a diagram provided in Figure 6. To begin the process, the lipid solution is deposited onto Indium Tin Oxide

(ITO) covered slides, and the chloroform is evaporated in a vacuum chamber. The desired solution to form the GUVs in (water, sucrose, etc.) is then deposited onto the dried lipids, sealed via a spacer and vacuum greased, and placed in an incubation chamber set to 50° C. An AC current (2.5 Volts peak to peak at 5 Hz) is then applied to the ITO slides, producing an electric field. The electric field causes the lipids to bleb off the ITO slides, forming GUVs in the solution.

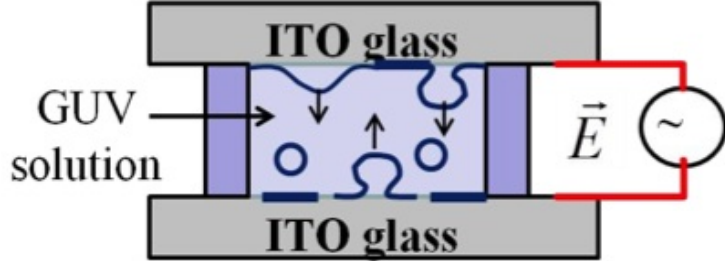


Figure 6: Electroformation diagram obtained from [12].

To achieve the refractive index difference needed for optical trapping, dialysis is conducted to swap the solution the GUVs are sitting in with one of equal osmotic pressure and lower refractive index. Dialysis is performed by taking the obtained GUV solution and pipetting it into a regenerated cellulose membrane pouch (MWCO 150,000) that allows transfer of solution, but keeps GUVs from escaping. The membrane is placed in a bath of a different solution that is several magnitudes greater in volume than the GUV solution, but with equal osmotic pressure. Diffusion takes place and solutions are swapped.

GUV trapping begins after dialysis is complete. After dialysis, the GUVs are filled with a solution that has a higher refractive index than what is outside the GUVs. The vesicle solution is placed inside the trap, and once the flow slows down, the vesicle is trapped. Once trapped, the power of the laser is increased, thus stretching the vesicle.

Figure 7 depicts what the stress profile felt by the GUV will be. This stress is calculated using Equation (3.1). Since stress is defined as $\sigma = \frac{F}{A}$, dividing by the cross-sectional area of the GUV will produce the stress. By doing this, we obtain

$$\sigma = \frac{F}{A} = \frac{n_1 Q(\alpha) P}{c A} = \frac{n_1 Q(\alpha) I(\alpha)}{c} \quad (4.2)$$

where α is the angle of incidence between the laser beam and the GUV's surface, and $I(\alpha)$ is the intensity of the laser at a certain incident angle. With this, stress values can be calculated as a function of incident angle using a simple Matlab code.

After successful trapping, images will be obtained of stretched vesicles. Image analysis will yield strain values of the GUVs. Numerically calculated stress values will be obtained

from Equation (4.2). Knowing stress and strain, quantities such as Young's Modulus and bending elasticity can be obtained, and will be compared to the work done by [12], with that author's results shown in Figure 8. Different bending elasticities as a function of lipid concentration will be obtained throughout the experiments. Studies showing how phase domains relocate as a function of curvature will also be done in the same manner.

Stress vs Incident Angle for two beams: Giant Unilamellar Vesicle

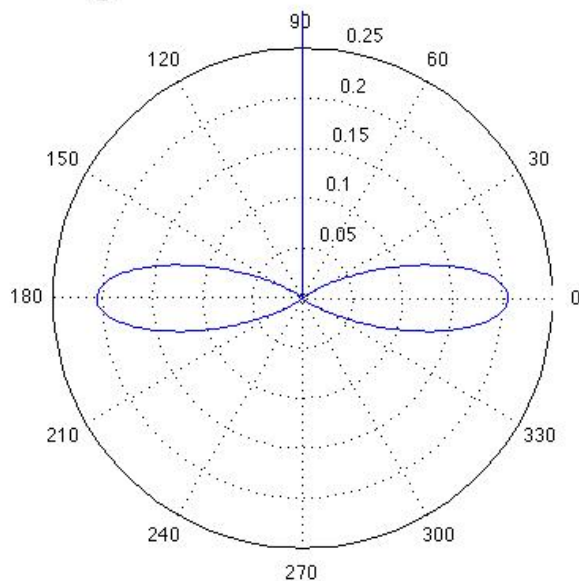


Figure 7: Stress profile for a trapped GUV. The inside is simulated as a sucrose solution, and outside is glucose. Refractive index difference is 0.02. The fiber separation distance is $100\ \mu\text{m}$, and the power is 100 mW.

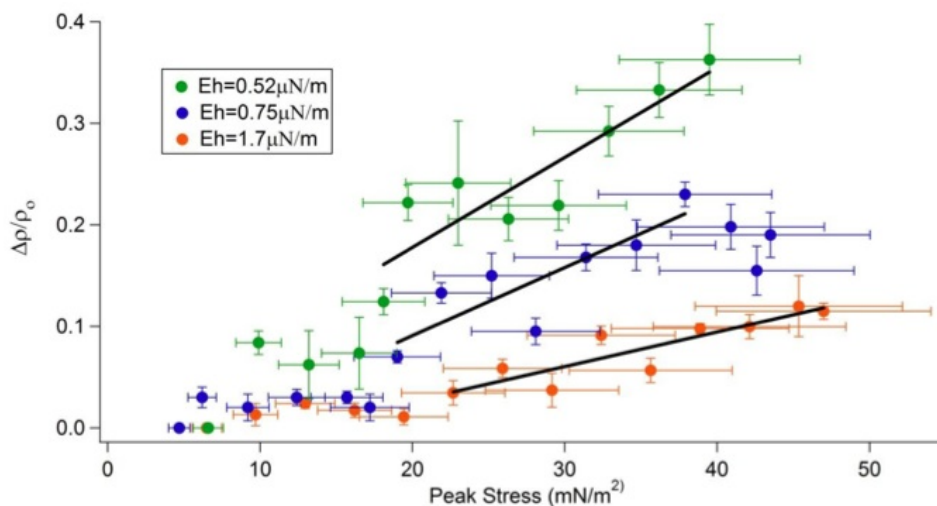


Figure 8: Strain vs Stress profiles of GUVs obtained from [12]. Green dots represent GUVs of radius $4.6\ \mu\text{m}$. Blue dots represent GUVs of radius $5.0\ \mu\text{m}$. Orange dots represent GUVs of radius $5.8\ \mu\text{m}$.

4.2 Project 2: Liquid Crystal Stretching

4.2.1 Background and Theory

Liquid crystal has been studied for uses in electronic devices such as LCD TVs, temperature sensors, and privacy windows. Recently, the Hirst group has studied liquid crystals for use as a medium for self-assembly of nano particles [20] and solar collectors [21]. The physics of liquid crystals have been an area of interest for nearly a century. For this work, how liquid crystals respond of optical forces is considered. The liquid crystal 5CB (4-cyano-4-n-pentylbiphenyl) is used for this study.

The liquid crystal 5CB, as shown in Figure 9, is a rod-like molecule that exhibits very interesting phase behavior [1]. As the name states, liquid crystals exhibit both liquid and crystalline phase behavior in the same phase. In this nematic phase, defects may exist. Defects, shown in Figure 9, occur when there is misalignment of the liquid crystal molecules. With its phase transitions well known, it makes an excellent candidate for studying nematic droplets.

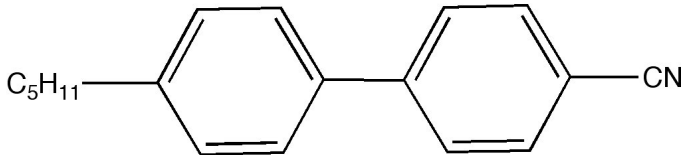


Figure 9: Diagram of 5CB molecule obtained from [2].

Nematic droplets have been studied extensively, both experimentally and theoretically. Experiments have done studying how defects occur in droplets, especially when polymers are introduced into the solution that holds the liquid crystal [4,22]. Theoretical studies have been done that predict how light will pass through different droplets of varying radii [23], as well as to properly predict the types of defects seen in thin films of nematic liquid crystal [24]. Different geometries of liquid crystal confinement have been studied, such as cylindrical cavities [25]. This leaves the door open to study how defects may change as a function of changing confinement geometry.

To successfully model any system of molecules, one must first begin by determining the ground state of molecular orientation. This is done by minimizing the Free Energy of the system. For a nematic liquid crystal, the free energy of the bulk system has been known for quite sometime, put together by Frank [26]. The Frank Free Energy of a nematic is given by

$$F = \int_V f dV \quad (4.3)$$

$$f = \frac{1}{2} [K_1 (\nabla \cdot \hat{n})^2 + K_2 (\hat{n} \cdot \nabla \times \hat{n})^2 + K_3 (\hat{n} \times \nabla \times \hat{n})^2] \quad (4.4)$$

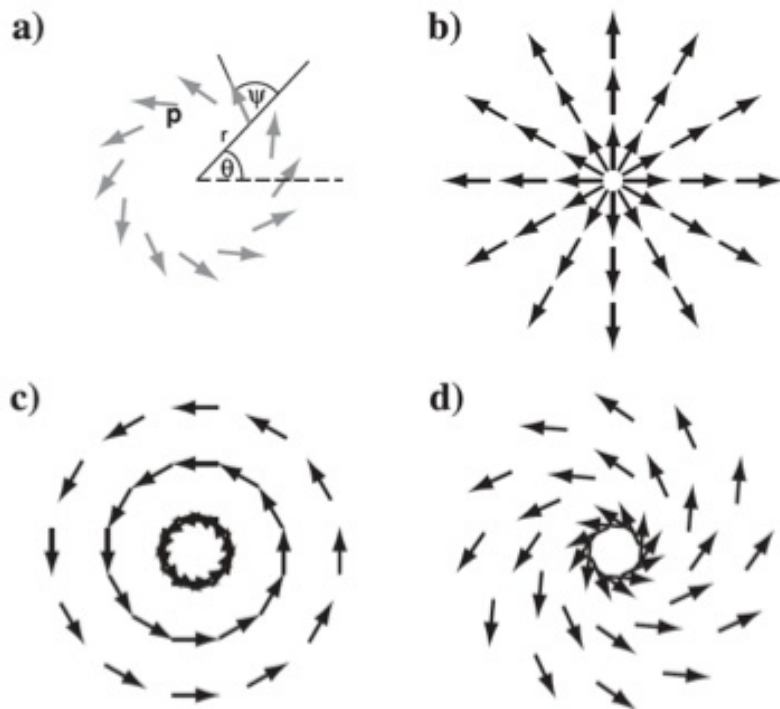


Figure 10: Director field diagrams obtained from [27]. (a) A point defect in polar coordinates. Different orientations for (b) aster, (c) vortex, and (d) spiral.

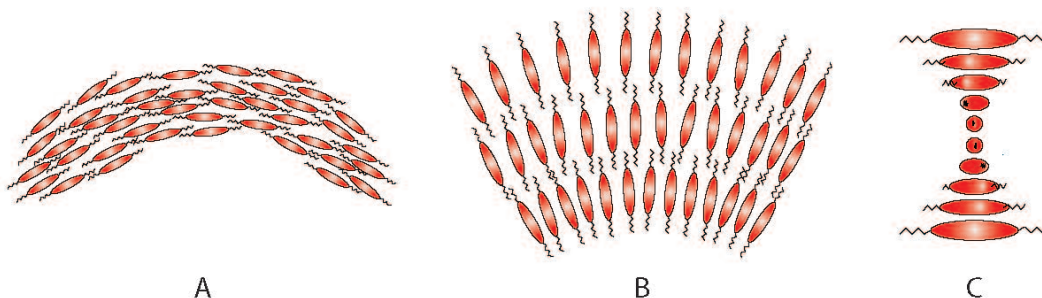


Figure 11: Diagrams of bend, splay, and twist, from left to right, respectively. Image was obtained from [2].

where K_1, K_2 , and K_3 are the splay, twist, and bend energy constants, respectively, (physical meanings are shown in Figure 11), and \hat{n} is the director unit vector. For surface interactions, there is the saddle-splay energy term, K_{24} . In the presence of an electric field, there is an additional component added to the energy, $-\frac{1}{2}\epsilon_0\Delta\epsilon(\vec{E} \cdot \hat{n})^2$, where ϵ_0 is the permittivity of free space and $\Delta\epsilon$ is the difference in permittivities between the possible orientations of the director.

The first goal of this project was to become acquainted with the theory and mathematics, so several equations were chosen to re-derive from a paper. The model begins by working in two dimensions. The director field, being a vector field, is parameterized as $\vec{n}(x, y) = n_x \hat{x} + n_y \hat{y}$. Since the director is a unit vector, and all directors are of the same magnitude, we do not care about the magnitude of \vec{n} , only its orientation. With this, we can work in a scalar field, $\theta = \theta(x, y)$, instead of a vector field. Thus the director can be rewritten as $\vec{n}(x, y) = \cos(\theta(x, y))\hat{x} + \sin(\theta(x, y))\hat{y}$ [24].

When minimizing the Frank Free Energy of a nematic, it is sometimes beneficial to make certain approximations. By setting $K_1 = K_2 = K_3 = K$, Equation (4.4) can be reduced to [23]

$$f = \frac{K}{2} [(\nabla \cdot \hat{n})^2 + (\nabla \times \hat{n})^2] \quad (4.5)$$

It is important to note that in 2D there are no twist contributions to the free energy, and also the surface energy terms to go zero. Substituting the director into Equation (4.5), including the electric field term, and assuming the electric field is in the x-direction, we obtain

$$f = \frac{K}{2} [\theta_x^2 + \theta_y^2 - \epsilon_0 \Delta \epsilon E^2 \cos^2(\theta)] \quad (4.6)$$

where $\theta_i = \frac{\partial \theta}{\partial x_i}$. Minimization of this equation comes via the Euler-Lagrange equation. After minimization the equation obtained is

$$\nabla^2 \theta - \frac{1}{\zeta^2} \sin(\theta) \cos(\theta) = 0 \quad (4.7)$$

where $\zeta = \frac{1}{E} \sqrt{\frac{K}{\epsilon_0 \Delta \epsilon}}$, and is known as the correlation length. Note that in the absence of an electric field, Equation (4.7) reduces to Laplace's equation for θ . This equation is a nonlinear differential equation, and the next step for this part of the project is to solve this equation to get the director configuration.

One may also avoid making the approximation of equal Frank constants. When doing this, it is beneficial to introduce two new constants: $J = \frac{K_1 + K_3}{2}$, and $D = \frac{K_1 - K_3}{2}$. J is an average of the constants, and measures the material's elastic isotropy. D measures the material's elastic anisotropy. Deem was the first to propose this method [28]. With these new constants and substituting them into Equation (4.4), we obtain

$$f = \frac{1}{2} [(J + D) (\nabla \cdot \hat{n})^2 + (J - D) (\hat{n} \times \nabla \times \hat{n})^2] \quad (4.8)$$

Substituting the expression for the director into the above equation, we get the free energy equation for a 2D nematic with unequal Frank constants not in the presence of an electric field:

$$f = \frac{J}{2} (\theta_x^2 + \theta_y^2) + \frac{D}{2} (\theta_y^2 - \theta_x^2) \cos(2\theta) - D\theta_x\theta_y\sin(2\theta) \quad (4.9)$$

Once again, we will minimize this equation to find the preferred director orientation. After minimization, we obtain

$$-J(\theta_{xx} + \theta_{yy}) + D(\theta_y^2 - \theta_x^2 + 2\theta_{xy})\sin(2\theta) + D(\theta_{xx} - \theta_{yy} + 2\theta_x\theta_y)\cos(2\theta) = 0 \quad (4.10)$$

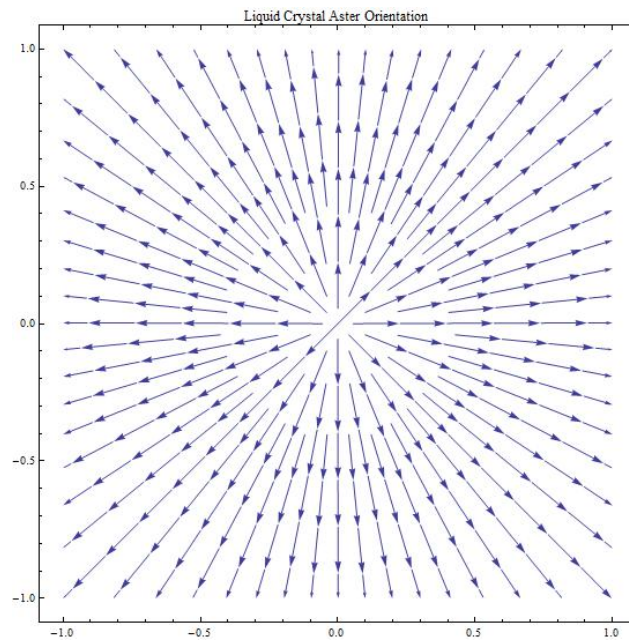
The solution to this equation is trivial: θ is equal to a constant. This corresponds to the molecules, on average, pointing in the same direction. While this is a valid solution, it does not show that there are any disclination lines present, even though disclinations can be present. To obtain more solutions, it is beneficial to introduce a polar coordinate system by defining $\theta(r, \phi) = s\phi + \psi(r, \phi)$. Here, s is referred to the disclination strength, and ϕ is the polar angle swept out with respect to the x-axis. The director is thus defined in polar coordinates as $\vec{n}(r, \phi) = \cos(\theta - s\phi)\hat{r} + \sin(\theta - s\phi)\hat{\phi} = \cos(\psi)\hat{r} + \sin(\psi)\hat{\phi}$. After transforming (9) to polar coordinates, we obtain for the minimized free energy

$$\begin{aligned} -J\left(\psi_{rr} + \frac{\psi_r}{r}\right) + D\left[(2s-1)\psi_{rr} + \frac{\psi_r}{r}\right]\cos(2(s-1)\phi + 2\psi) + \\ + D\left[\frac{s(s-2)}{r^2} - \psi_r^2\right]\sin(2(s-1)\phi + 2\psi) = 0 \end{aligned} \quad (4.11)$$

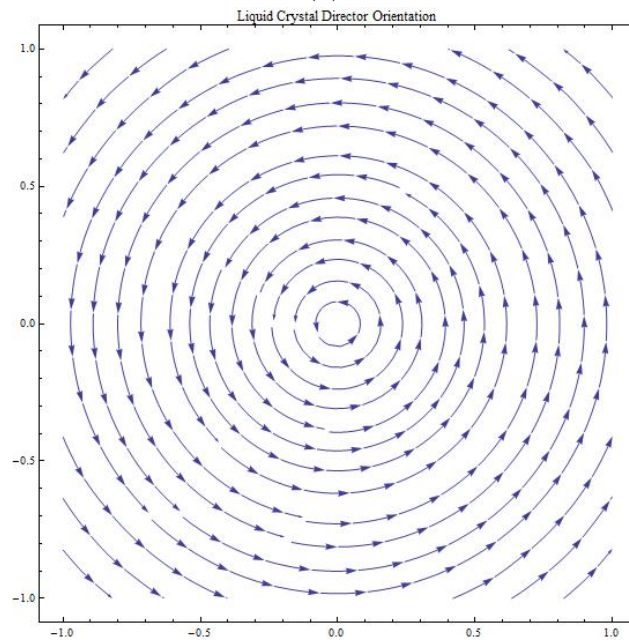
with the assumption that ψ has no angular dependence. This is a very important equation. By choosing different s values that correspond to different disclination strengths, we can obtain various director configurations. Let $s = 1$. Equation (4.11) becomes

$$-(J - D\cos(2\psi))\left[\psi_{rr} + \frac{\psi_r}{r}\right] - D\left[\psi_r^2 + \frac{1}{r^2}\right]\sin(2\psi) = 0 \quad (4.12)$$

Solutions to this equation are $\psi = 0, \pi$ which correspond to aster patterns. $\psi = \pm\frac{\pi}{2}$ produce vortex patterns. Solutions are plotted in Figure 12. The next step in this portion of the project is to see how these orientations may change when subjected to an elliptical geometry. This will be done by solving for the free energy in Equation (4.3) in a elliptical geometry. This will produce a free energy as a function of the eccentricity of the ellipse. Minimizing the free energy as a function of the eccentricity will then reveal the shape the droplet will take.



(a)



(b)

Figure 12: Possible orientations of the director \hat{n} found from the solutions of Equation (4.12). (a) Aster pattern. (b) Vortex pattern.



Figure 13: Liquid crystal droplets as seen between cross polarizers. Scale bar is 50 μm .

4.2.2 Methods and Proposed Work

The theory proposed in the previous section is developed to compliment the upcoming proposed experiment. For this experiment, a nematic droplet is to be placed inside the dual-fiber optical trap and stretched into an ellipsoid. This will lead to a better understanding how nematics behave when exposed to a variety of different forces.

To prepare for the experiment, the droplets of nematic liquid crystal must be formed. To prepare the nematic droplets, the liquid crystal 5CB is deposited into a polymer solution composed of 1 wt% polyvinyl alcohol (PVA) that is heated well above the isotropic temperature of the liquid crystal (35°C). The purpose of the polymer is to prevent coalescence of the liquid crystal and maintain droplet formation. Droplets of 5CB are formed in the PVA solution by stirring the liquid crystal rapidly by hand for several minutes. Figure 13 shows prepared liquid crystal droplets.

As stated in Section 3, there must be a difference in refractive indices between material and solution to ensure trapping. More specifically, the object being trapped must have a higher refractive index than the solution it is sitting in. 5CB has two refractive indices, one for each possible orientation of the molecule. The ordinary refractive index, n_o , is 1.53567. The extraordinary refractive index, n_e , is 1.71439. With these high refractive indices compared to the refractive index of the surrounding solution, which is about that of pure water (1.33), trapping will occur.

However, probing the droplet for mechanics properties has been a difficult task. As refractive index plays a role in trapping an object, droplet diameter also plays a role in how the droplet will be stretched. I have been seen experimentally that droplets less than 10 μm in diameter will not undergo stretching when the laser power output is increased. This is due to the stress distribution on the droplet. To achieve optimal stress distribution that will induce stretching, I have determined that the droplets must be at least 20 μm in diameter. This was done by running the Matlab stress profile program with changing diameters until an ideal profile was achieved. Figure 14 shows a successful trapping of a nematic droplet in water. Figure 15 shows the corresponding stress profile of the trapped droplet. The stress is distributed around the poles of the droplet, and no stretching occurred. Calculations have shown that droplets with a diameter of 20 μm or more will produce ideal stress profiles.

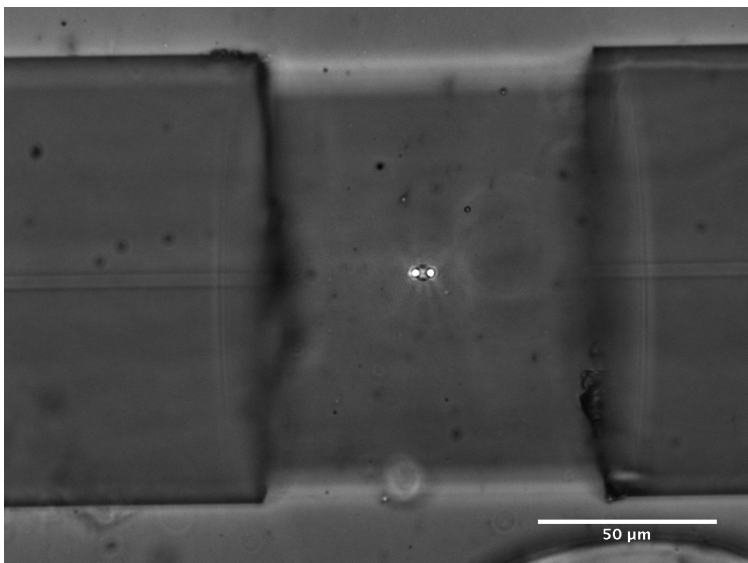


Figure 14: Trapped liquid crystal droplet. The droplet diameter is roughly $4.88 \pm 0.01 \mu\text{m}$. Fiber separation distance is $96.32 \mu\text{m}$. Laser power is 100 mW.

Stress vs Incident Angle for two beams: Liquid Crystal Droplet

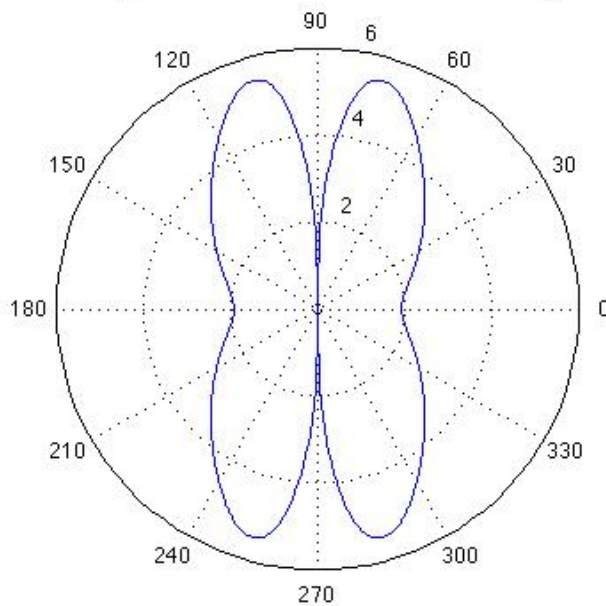


Figure 15: Stress profile for 5CB droplet in water, complementing Figure 14. The ordinary refractive index is used for 5CB, and the refractive index of water is 1.33.

4.3 Project 3: Particle Orientation and Surface Curvature

4.3.1 Theory and Background

The final experiment to be conducted concerns how curved surfaces and particles on those surfaces are linked. This project began with interest in looking at Pickering emulsions. Pickering emulsions are emulsions that are stabilized by particles acting as a surfactant. While trying to create Pickering emulsions, bijels were seen to form [29, 30]. Bijel stands for "bi-continuous interfacially jammed emulsion gel." Viewing these bijels led to an idea to study how soft structures form, as well as different types of particles could influence the curvature of the interface. I have produced several different soft structures from oil and water combinations stabilized by particles, as shown in Figure 16. The data obtained from the experiment will also allow us to create correlation functions for mapping particles in 3D space, with the possibility of developing techniques applicable to other systems.

How effectively these particles stabilize the oil/water mixture depends on certain criteria such as particle size, wettability, and the level of particle interaction. The effectiveness of how these particles stabilize the emulsion is rationalized as the attachment energy, E [31]. This attachment energy is given by

$$E = \pi R^2 \gamma_{ow} (1 + \cos(\theta))^2 \quad (4.13)$$

where R is the radius of the particle, γ_{ow} is the interfacial tension between oil and water, and θ is the contact angle of the particle. From Equation (4.13), when $\theta = 90^\circ$, the attachment energy is at a minimum, and the mixture will be perfectly stable.

4.3.2 Methods and Proposed Work

The particles used are latex particles provided by the Mitragoti Lab at the University of California, Santa Barbara. The particles begin as spheres with a diameter of 1 μm , and then are stretched to varying aspect ratios (AR) of 1.5, 2, and 3 using a film stretching method [32]. The particles have the fluorophore FITC (fluorescein isothiocyanate) on the inside, and have a zeta potential between 40-50 mV. The zeta potential is the electrical potential between the stationary fluid at the surface of the particle, and the surrounding fluid. It is a measure of the stability of the particle in solution.

For analysis of particles on curved surfaces, 2D and 3D image stacks will be obtained from different emulsion samples via confocal microscopy. Free multiple particle detection software (Particle tracker) will be used to locate particles in space and create correlation functions. Surface mapping is a collaboration with Tim Atherton's theoretical soft matter group at Tufts University. By providing Professor Atherton with image stacks of the soft structures, surface mapping will be computed via his algorithms that connect particle packing and orientation to surface structure.

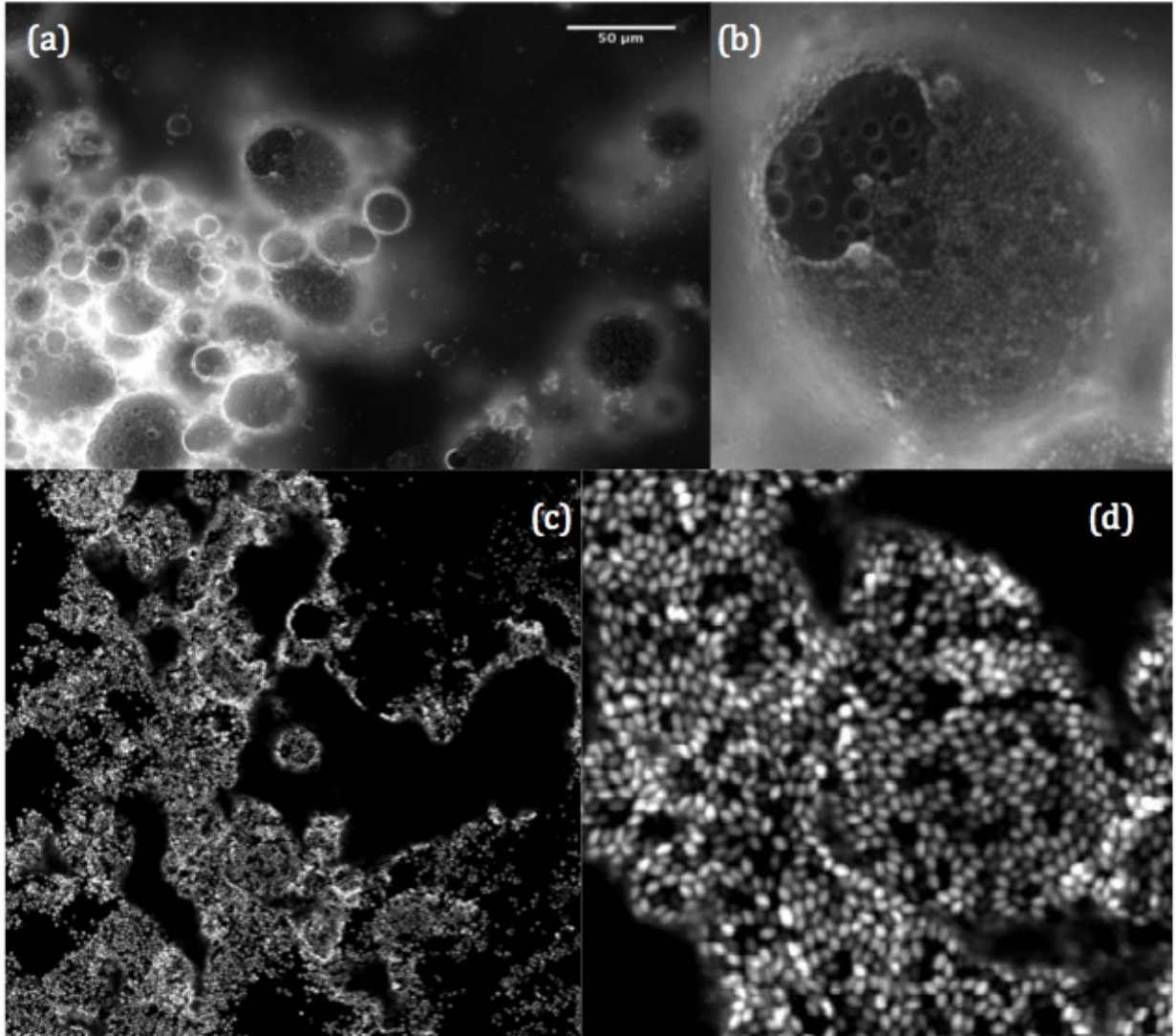


Figure 16: Various soft structures from via emulsions of water and oil with particles as the surfactant. (a) and (b) are formed with $AR=1$ particles (spheres). (c) and (d) are formed with $AR=1.5$ particles (ellipses). The oil to water ratio was 50/50.

5 Conclusions and Timeline

Several experiments have been proposed to study the effect of inducing curvature on condensed matter systems and seeing their effects. For giant unilamellar vesicles, inducing curvature will lead to knowing whether different lipid phase domains will prefer sites of extreme curvature or minimal curvature. During this experiment, the mechanical properties of the membrane will be studied to see if current stress-strain relations hold in the extreme elastic regime. Curvature of a nematic droplet will also be studied. Mechanical properties will be investigated, as well as possible molecular configurations. Theoretical studies will be done to complement the experiment. Curvature of pickering emulsions and bijels formed via particles at the interface of oil and water will also be investigated.

In conclusion, these studies will aid in the understanding of curvature's roles in condensed matter systems. Knowing how certain materials behave will aid in the production of many different materials, as well as the control needed to produce such things. And most importantly, they will lead to an increase in knowledge of many different physical systems.

Experiment	Year 1	Year 2	Year 3
Single Lipid GUV Production and Trapping	X	X	
Two Lipid GUV Production and Trapping	X	X	
Nematic Droplet Trapping	X		X
Nematic Droplet Theory Work	X	X	X
Curvature Related to Particles on Curved Surfaces	X	X	X

References

- [1] Chaikin, P.M. and Lubensky, T.C. *Principles of condensed matter physics*. Cambridge University Press, Cambridge, UK, 1997.
- [2] Hirst, L.S. *Fundamentals of Soft Matter Science*. CRC Press, Florida, 2012.
- [3] Nir, S., Wilschut, J. and Bentz J. The rate of fusion of phospholipid vesicles and the role of bilayer curvature. *Biochemica and Biophysica Acta*, **688**, 1982, 275-278.
- [4] Fernandex-Nieves, A. et al. Topological changes in bipolar nematic droplets under flow. *Physical Review Letters*, **98**, 2007, 087801.
- [5] Svoboda, V. and Block, S. M. Force and velocity measured for single kinesin molecules. *Cell*, **77**, 1994, 773-784.
- [6] Block, S.M. et al. Stretching DNA with optical tweezers. *Biophysical Journal*, **72**, 1997, 1335-1346.
- [7] Constable, A. et. al. Demonstration of a fiber-optical light-force trap. *Opt. Lett*, **18**, 1993, 1867-1869.
- [8] Guck, J. et. al. Optical Deformability as an Interent Cell Marker for Testing Malignant Transformation and Metastatic Competence. *Biophysical Journal*, **88**, 2005, 3689-3698.
- [9] Guck, J. et. al. The optical stretcher: a novel laser tool to micromanipulate cells. *Biophysical Journal*, **81**, 2001, 767-784.
- [10] Povinelli, M. L. et. al. Optical stretching of giant unilamellar vesicles with an integrated dual-beam optical trap. *Biomedical Optics Express*. **3**, 2012, 2419-2427.
- [11] Nichols, M. G. et. al. Determination of cell elasticity through hybrid ray optics and continuum mechanics modeling of cell deformation in the optical stretcher. *Applied Optics*, **48**, 2009, 6344-6354.
- [12] Piñòn, T. M. Fiber based dual-beam optical trapping platform for stretching lipid vesicles. Ph.D. Dissertation, University of California, Merced, 2013.
- [13] Lincoln, et al. Reconfigurable microfluidic integration of a dual-beam laser trap with biomedical applications. *Biomedical Devices*, **9**, 2007, 703-710.
- [14] Cicuta, P., Keller, S., and Veatch, S. L. Diffusion of liquid domains in lipid bilayer membranes. *Cond. Soft Matter*, 2012.
- [15] Yuan, J., Hira, S. M., Strouse, G. F., and Hirst, L. S. Lipid bilayer disks and banded tubules: photoinduced lipid sorting in ternary mixtures. *J. AM. CHEM. SOC.* **130**, 2008, 2067-2072.

- [16] Schmidt, M. L. et al. Phase equilibria in DOPC/DPPC: Conversion from gel to sub gel in two component mixtures. *The Journal of Chemical Physics*, **131**, 2009, 175103.
- [17] Veatch, S. L. and Keller, S. L. Separation of Liquid Phases in Giant Vesicles of Ternary Mixtures of Phospholipids and Cholesterol. *Biophysical Journal*. **85**, 2003, 3074-3083.
- [18] Groves, J. T. Bending Mechanics and Molecular Organization in Biological Membranes. *Annu. Rev. Phys. Chem.*, **58**, 2007, 697-711.
- [19] Helfrich, W. and Servuss, R. M. Undulations, steric interaction and cohesion of fluid membranes. *Nuovo Cimento*, **3**, 1984, 137-151.
- [20] Rodarte, A. L. et al. Tuning quantum dot organization in liquid crystal for robust photonics applications. *Chem. Phys. Chem.*, **15**, 2014, 1413-1421.
- [21] Rodarte, A. L. et al. Dye sensitized cholesteric liquid crystalline photonic luminescent solar concentrator. *Liquid Crystals*, 2014.
- [22] Lopez-Leon, T. and Fernandez-Nieves, A. Drops and shells of liquid crystals. *Colloid Polym. Sci.*, **289**, 2011, 345-359.
- [23] Zumer, S. and Doane, J. W. Light scattering from a small nematic droplet. *Physical Review A*, **34**, 1986, 3373-3386.
- [24] Hartnett, G. Spiral Patterns in Liquid Crystals. *Syracuse University Honors Program Capstone Projects*, 2009, Paper 463.
- [25] Faetti, S. The effects of curvature on nematic liquid crystals confined in a cylindrical cavity. *Physical Letters A*, **237**, 1998, 264-270.
- [26] Frank, F. C. 1. Liquid Crystals. On the theory of liquid crystals. 1958, 19-28.
- [27] Kruse, K. et al. Asters, vortices, and rotating spirals in active gels of polar filaments. *Physical Review Letters*, **92**, 2004, 078101.
- [28] Deem, M. W. Disclination asymmetry in two-dimensional nematic liquid crystals with unequal Frank constant. *Physical Review E*, **54**, 1996, 6441-6451.
- [29] White, K. A. et al. Influence of particle composition and thermal cycling on bijel formation. *Condensed Soft Matter*, 2008.
- [30] Herzig, E. M et al. Bicontinuous emulsions stabilized solely by colloidal particles. *Nature Materials*, **6**, 2007, 966-971.
- [31] Prestidge, C. A. and Simovic, S. Nanoparticle encapsulation of emulsion droplets. *International Journal of Pharmaceutics*, **324**, 2006, 92-100.

- [32] Champion, J., Katare, Y., and Mitragotri, S. Making polymeric mirco- and nanoparticles of complex shapes. *Proceedings of the National Academy of Sciences of the United States*, **104**, 2007, 11901-11904.